Increased persistent Na^+ current and its effect on excitability in motoneurones cultured from mutant SOD1 mice

J. J. Kuo[1,2], T. Siddique[2,3], R. Fu[3] and C. J. Heckman[1,2,4]

Departments of [1]Physiology, [2]Institute for Neuroscience, [3]Neurology and [4]Physical Medicine and Rehabilitation, Northwestern University Feinberg School of Medicine, Chicago, IL 60611, USA

Mutations in the enzyme superoxide dismutase 1 (SOD1) initiate a progressive motoneurone degeneration in amyotrophic lateral sclerosis (ALS). Transgenic mice overexpressing this mutation develop a similar progressive motoneurone degeneration. In spinal motoneurones cultured from presymptomatic mice expressing the glycine to alanine mutation at base pair 93 (G93A) SOD1 mutation, a marked increase in the persistent component of the Na^+ current was observed, without changes in passive properties. This increase only enhanced neuronal excitability in high input conductance cells, as low input conductance cells exhibited a compensatory outward shift in the current remaining after Na^+ blockade. High input conductance motoneurones tend to be large, so these results may explain the tendency of large motoneurones to degenerate first in ALS. Riluzole, at the therapeutic concentration used to treat ALS, decreased neuronal excitability and persistent Na^+ current in G93A motoneurones to levels observed in the control motoneurones. Aberrations in the intrinsic electrical properties may be among the first symptoms to emerge in SOD1-linked ALS.

(Received 18 August 2004; accepted after revision 11 January 2005; first published online 13 January 2005)
Corresponding author C. J. Heckman: Department of Physiology, Northwestern University Feinberg School of Medicine, 303 E. Chicago Ave, Chicago, IL 60611, USA. Email: c-heckman@north-western.edu

Amyotrophic lateral sclerosis (ALS) is usually a fatal neurodegenerative disease involving motoneurone degeneration. Patients with mutations in the enzyme superoxide dismutase 1 (SOD1) account for approximately 20% of all familial ALS cases (Deng *et al.* 1993; Rosen *et al.* 1993; Siddique & Lalani, 2002). Transgenic mice overexpressing a mutated human SOD1 gene develop a progressive neurodegeneration similar to SOD1-linked ALS in humans (Siddique, 1991; Gurney *et al.* 1994), with muscle weakness leading to paralysis (Kong & Xu, 1998). Additionally, spinal motoneurones from SOD1 transgenic mice acquire pathological features seen in patients, such as axonal spheroids (Dal Canto & Gurney, 1997) and fragmentation of the Golgi apparatus (Mourelatos *et al.* 1996). Results from studies using mutant SOD1 mice support the hypothesis that mutant SOD1 confers a toxic gain of function rather than an enzymatic loss of function. Despite nearly normal levels of SOD1 enzymatic activity, mutant SOD1 mice develop ALS, whereas SOD1 knockout mice do not (Gurney *et al.* 1994; Reaume *et al.* 1996; Wong *et al.* 2002).

The nature of the SOD1 gain of function has yet to be identified, but motoneurone vulnerability to excitotoxicity may be important. Studies have focused on glial glutamate transport, glutamate receptors and calcium buffering (Palecek *et al.* 1999; Beers *et al.* 2001; Cleveland & Rothstein, 2001; Rao & Weiss, 2004). However, intrinsic motoneurone excitability may also be a major contributor to excitotoxic vulnerability. Calcium enters the motoneurone not only through glutamate receptors during synaptic transmission, but also during each action potential through voltage-dependent Ca^{2+} channels (Powers & Binder, 2001). Thus, cells that generate a greater number of action potentials per unit of input are more excitable and likely to be more vulnerable to excitotoxicity.

Cultured motoneurones from presymptomatic mutant SOD1 mice, in fact, were characterized by enhanced intrinsic excitability, with a marked increase in the slope of the relation between the firing frequency (F) and injected current (I) (Kuo *et al.* 2004; Pieri *et al.* 2003). Many intrinsic motoneurone properties can affect the gain of the F–I function, including the afterhyperpolarization (AHP), Ca^{2+} currents and input conductance (Rekling *et al.* 2000; Powers & Binder, 2001). In addition, persistent currents (PCs) have a major impact on F–I gain (Hounsgaard *et al.* 1988; Hounsgaard & Kiehn, 1989; Bennett *et al.* 1998; Lee & Heckman, 1998). Although an L-type Ca^{2+}

 DOI: 10.1113/jphysiol.2004.074138

channel plays an important role in generating these PCs (Hounsgaard & Kiehn, 1989; Perrier & Hounsgaard, 2003), a persistent Na^+ current (PC_{Na}) is also important (Lee & Heckman, 1999; Li & Bennett, 2003). Moreover, PC_{Na} is likely to be essential for spike generation during sustained inputs and thus should strongly influence *F–I* gain (Lee & Heckman, 2001). Riluzole, a drug that slows the course of ALS in mutant SOD1 mice (Gurney *et al.* 1996) and human patients (Bensimon *et al.* 1994), is in fact a selective blocker of PC_{Na} at low concentrations (Urbani & Belluzzi, 2000).

We therefore tested the hypothesis that mutant SOD1 motoneurones have increased levels of PC_{Na}. We further examined the role of PC_{Na}. By pharmacologically inhibiting PC_{Na}, we observed a marked decrease in excitability and PC_{Na}. These results suggest that PC_{Na} may play a direct role in motoneurone degeneration. Some of this work has been previously published in abstract form (Kuo *et al.* 2002).

Methods

All procedures were approved by the Northwestern University animal care and use committee.

Mice

Transgenic mice expressing the mutant (G93A) and wild-type human SOD1 gene were bred and maintained in barrier facilities. Mice overexpressing the G93A SOD1 mutation began to demonstrate clinical symptoms (tremors) at approximately 200 days old. Transgenic G93A mice represent an excellent model for the study of ALS, as many pathological and phenotypic symptoms resemble those observed in human patients (Mourelatos *et al.* 1996; Dal Canto & Gurney, 1997; Gurney, 1997; Kong & Xu, 1998; Bruijn *et al.* 2004). The control sample consisted of wild-type SOD1 and non-transgenic embryos from the human wild-type SOD1 mice. No statistical difference was observed in any parameter between these two samples, so they were combined as the control sample. Standard PCR techniques, as previously described, were used to identify the genotype of each embryo (Deng *et al.* 1993; Gurney *et al.* 1994). For part of the studies of riluzole inhibition, standard inbred C57BL6 (Harlan, Indianapolis, IN, USA) mouse embryos were used.

Cell culture

The spinal cord was removed, dissociated and cultured from embryonic mice at day 12–14, with some modifications (Anelli *et al.* 2000). After killing the pregnant mouse with an overdose of isoflurane followed by decapitation, each embryo was placed in an individual Petri dish containing cold Neurobasal-A medium (Invitrogen, Carlsbad, CA, USA). Each spinal cord was quickly removed and sliced into 400-μm slices. The dissociation and cell isolation of the spinal cord slices have been previously described (Levi *et al.* 1989). The dissociated cells were plated at approximately 130 000 cells cm^{-2} on glass coverslips coated with poly-D-lysine. The initial medium contained Neurobasal-A medium (Invitrogen), B27 Supplement (Invitrogen), 1% penicillin-streptomycin, 1 mM L-glutamine and an additional 2 mg ml^{-1} glucose. The plating medium contained the initial medium plus 15% heat-inactivated horse serum. The plating medium was changed after 2 days *in vitro* to a serum-free maintenance medium containing the initial medium with 20 ng ml^{-1} nerve growth factors (Invitrogen). The maintenance medium was replaced every 3–4 days and cultures were used between 10 and 30 days *in vitro*.

Electrophysiology

Electrodes were typically 3–4 MΩ in resistance when filled with a solution containing (mM): potassium gluconate 145, $CaCl_2$ 0.1, EGTA 1.1, Hepes 5, $MgCl_2$ 2, and ATP-Mg^{2+} 5; with a pH of 7.3. Artificial cerebrospinal fluid (aCSF) contained (mM): NaCl 138.5, $NaHCO_3$ 28.8, NaH_2PO_4 1.1, KCl 3.3, $MgSO_4$ 1.6, $CaCl_2$ 2.8, glucose 11, picrotoxin 0.1 (Sigma, St Louis, MO, USA), 2,3-Dioxo-6-nitro-1,2,3,4, -tetrahydrobenzo[f]quinoxaline-7-sulfonamide disodium salt (NBQX) 0.01 (Tocris, Ellisville, MO, USA), strychnine 0.01 (Sigma) and D-(-)-2-Amino-5-phosphonopentanoic acid (AP5) 0.1 (Tocris); with a pH of 7.4 when bubbled with 95% O_2–5% CO_2. TTX was added to the aCSF as a 1 μM TTX solution. Riluzole was dissolved in DMSO and added to the aCSF as a 0.05% DMSO solution. Vehicle control experiments showed no differences. All aCSF and drug solutions were applied to the bath. Data were acquired at 10 kHz using a 1401 Plus (Cambridge Electronics Design) and digitally filtered off-line.

Whole-cell recordings

Whole-cell patch-clamp measurements were performed at room temperature using the Axoclamp 2A or Multiclamp 700A amplifier (Axon Instruments, Union City, CA, USA). Current–voltage (*I–V*) relations were generated using ramp voltage commands lasting 5 s. Voltage returned to baseline at the same rate as the ascending phase in all experiments. These slow ramps have been previously shown to provide a good estimate of the motoneurone steady-state *I–V* behaviour (Lee & Heckman, 1998). The relationship between action potential firing frequency and current was measured with triangular injected current waveforms, lasting 5 s each for the ascending and descending phases. Motoneurones were selected based on the presence of a multipolar cell body and a soma size greater than 25 μm in diameter (Carriedo *et al.* 1996).

Data analysis

Data were analysed off-line using IGOR Pro software (Wavemetrics, Lake Oswego, OR, USA). The input conductance of the cell was determined by fitting a linear regression to the *I–V* relation in its linear region, subthreshold to the voltage-sensitive currents (Powers & Binder, 2001). The leak conductance was subtracted from each waveform to produce the leak-subtracted *I–V* relation. An inward PC was readily apparent in each cell as a progressive downward deviation in the leak subtracted *I–V* function (Fig. 1*C*). This PC reflected the interaction between two basic components, which were revealed by TTX application. PC_{Na} was measured as the difference between the raw *I–V* function and the function with TTX present (Fig. 1*D*). The difference between the zero level and the current remaining after TTX administration was defined as $PC_{TTX\text{-}ins}$. The amplitudes of the total PC, PC_{Na} and $PC_{TTX\text{-}ins}$ were measured as the integral of current with respect to voltage from 13 to 7 mV (Fig. 1*C* shaded region) hyperpolarized to the action potential voltage threshold, which was assessed from the first spike on the ascending phase of the *F–I* function. Our goal in referencing PC_{Na} and $PC_{TTX\text{-}ins}$ measurements to spike voltage threshold was to focus these measurements to the voltage region where these currents have a strong impact on the genesis of rhythmic firing during the *F–I* function (Lee & Heckman, 2001; Powers & Binder, 2001).

As in our previous study (Kuo *et al.* 2004), the *F–I* function provided an overall measurement of the neuronal steady-state excitability. The slope of the linear regression fitted to the ascending phase was defined as the *F–I* gain. The current thresholds were defined as the absolute current amplitude at the initial and final spike on the ascending and descending phases, respectively, of the current ramp protocol (see Fig. 3). The rate of rise of the action potential was calculated by dividing the time from spike threshold to action potential peak from this change in voltage. All other measurements for action potential properties were previously described (Kuo *et al.* 2004).

Student's *t* test was used to test for a significant difference of the means between the G93A cell sample and the control cell sample. A probability of < 0.05 was accepted as significant. Only data with consistent resting membrane potentials, holding current and spike overshoot were used.

Results

Up-regulation of persistent Na^+ currents

In all cells recorded, embryos were identified as positive or negative for containing the human SOD1 gene (either wild-type or G93A) using standard PCR techniques (Deng *et al.* 1993; Gurney *et al.* 1994). The G93A sample consisted of 33 cells. The control sample consisted of 27 cells (15 over-expressors of wild-type SOD1 and 12 non-transgenic from the wild-type SOD1 mice). As no significant differences were observed between the wild-type and non-transgenic samples, they were combined as the control sample.

The basic *I–V* functions resulting from the triangular commands are illustrated in Fig. 1. In some cells, a strong inward PC produced a negative slope region followed by one or more spikes probably initiated in the dendrites or axon, as the voltage commands showed little or no deviation due to a loss of clamp control (Fig. 1*A*). The addition of TTX eliminated the negative slope and spikes, indicating that the inward voltage-dependant conductance was PC_{Na} and the spikes were dependent on Na^+ rather than Ca^{2+}. The leak-subtracted records (Fig. 1*C*) are

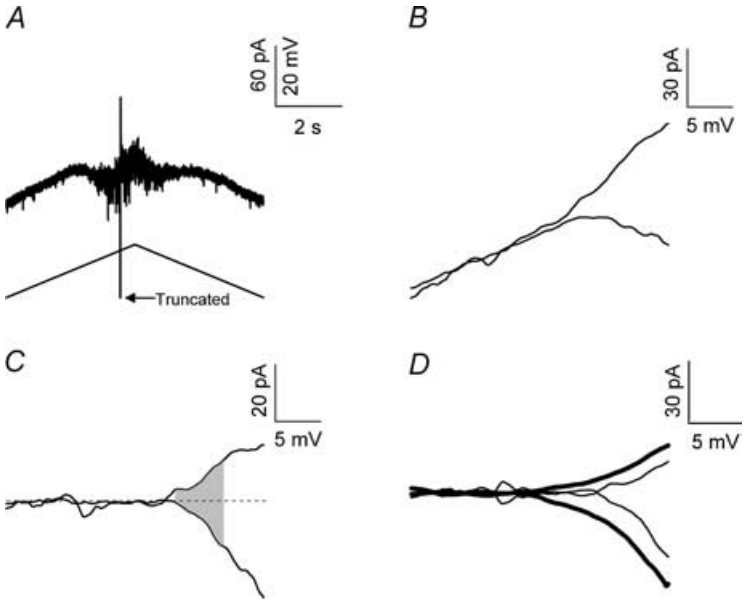

Figure 1. Current response to a voltage ramp
A, the current response (top) from a voltage command (bottom) is shown with a single unclamped spike. Cell was held at −82 mV. *B*, the *I–V* relation (ascending ramp only) is shown for a pre-TTX (downward trace) and TTX trial (upward trace). *C*, leak-subtracted *I–V* relations are shown for pre-TTX and TTX trials. The shaded area represents the voltage region for PC integration (with respect to 0 pA, dashed line). *D*, leak-subtracted currents are shown for control (thin lines) and G93A (thick lines) cells. The downward currents are the subtraction of the TTX trial ($PC_{TTX\text{-}ins}$) from pre-TTX and represents PC_{Na}.

shown as well as the subtraction of the TTX record from control to reveal PC_{Na} (Fig. 1*D*). Note that PC_{Na} and $PC_{TTX\text{-}ins}$ were larger in the G93A motoneurone (Fig. 1*D*).

Although the PC_{Na} magnitude exhibited considerable scatter in both control and G93A cell samples, it nonetheless tended to be substantially larger in G93A than control motoneurones ($P = 0.0001$) (Fig. 2*A*). However, PC_{Na} onset showed no significant differences (G93A, -60.7 ± 4.5 mV; control, -59.4 ± 5.4 mV; $P > 0.3$). As reported previously (Crill, 1996), PC_{Na} activation began at a level approximately 10 mV depolarized with respect to the resting membrane potential; this activation voltage level was hyperpolarized with respect to the spike voltage threshold (Table 1). Overall, these results support the hypothesis that the SOD1 mutation is associated with an increase in the magnitude of PC_{Na}.

Changes in TTX-insensitive persistent currents

Although we intended to focus on PC_{Na}, $PC_{TTX\text{-}ins}$ was also found to be significantly larger in the G93A sample ($P < 0.05$), though this difference (~26 pA) was smaller than for PC_{Na} (~51 pA) (Fig. 2*B*). The larger outward current of the G93A motoneurones was surprising because this would normally be associated with a decrease in neuronal excitability. This difference in $PC_{TTX\text{-}ins}$ was probably not due solely to changes in an outward current. In about 22% (6/27) of the control cells, $PC_{TTX\text{-}ins}$ was net inward, compared to 6% (2/33) of the G93A cells (Fig. 2*B*). Thus $PC_{TTX\text{-}ins}$ probably consisted of a mixture of Ca^{2+} and K^+ currents in most cells, suggesting that the net shift in the outward direction for $PC_{TTX\text{-}ins}$ in the G93A cells could be due to either an increased outward current or a decreased inward current.

Combined effects of persistent Na^+ and persistent TTX-insensitive currents

Together, PC_{Na} and $PC_{TTX\text{-}ins}$ defined the amplitude of the total PC. In nearly all G93A and control cells after leak subtraction, this PC was net inward (G93A, $n = 32/33$; control, $n = 25/27$). However, Fig. 2*C* illustrates that the PC magnitude was not significantly larger in the G93A motoneurones compared to control cells ($P > 0.05$). This lack of difference was due to the larger $PC_{TTX\text{-}ins}$ offsetting the larger PC_{Na} in the G93A motoneurones.

Differences in excitability of low- and high-input conductance cells

The effects of the SOD1 mutation on PC_{Na} and $PC_{TTX\text{-}ins}$ in relation to cell excitability were further studied by dividing the samples into low- and high-input conductance groups. Input conductance, which is proportional to soma size, is an especially important parameter for motoneurones (Powers & Binder, 2001), because it is a major determinant of their threshold for activation (i.e. recruitment) in

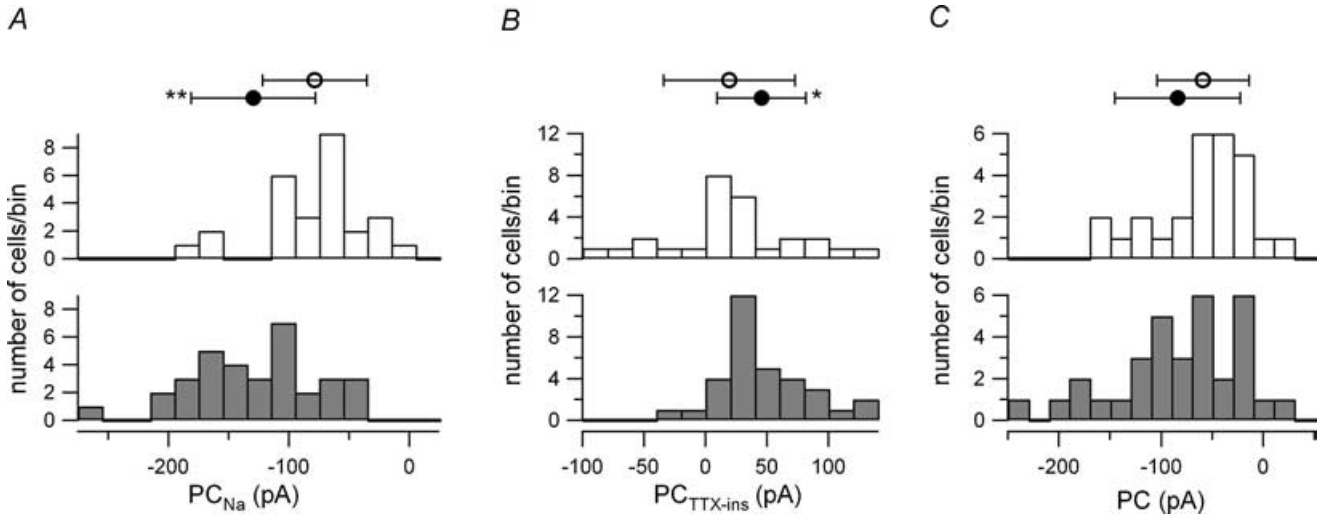

Figure 2. Increased PC_{Na} and $PC_{TTX\text{-}ins}$ in G93A motoneurones
A, PC_{Na} was significantly larger in G93A motoneurones (●) than from control cells (○). The shaded histogram represents the number of G93A motoneurones and the unshaded histogram was the number of control cells: G93A, -129.49 ± 51.48 pA; control, -78.41 ± 43.32 pA. *B*, $PC_{TTX\text{-}ins}$ was significantly larger in G93A motoneurones (●) than from control cells (○): G93A, 45.77 ± 36.11 pA; control, 19.47 ± 53.35 pA. *C*, the PC was similar between G93A (●) and control cells (○), due to a larger outward $PC_{TTX\text{-}ins}$ offsetting the larger PC_{Na} in the G93A cells: G93A, -83.71 ± 61.31 pA; control, -58.94 ± 45.10 pA. In each panel, the histogram was divided into 20-pA bins and the top symbols represent the mean ± S.D., $^*P < 0.05$ and $^{**}P < 0.0001$.

Table 1. Motoneurone passive and action potential properties

	Control			G93A		
	All ($n = 27$)	Low Gn ($n = 15$)	High Gn ($n = 12$)	All ($n = 33$)	Low Gn ($n = 16$)	High Gn ($n = 17$)
Input conductance (nS)	3.8 ± 2.0	2.1 ± 0.6	5.1 ± 1.6	3.7 ± 1.9	2.2 ± 0.7	5.0 ± 1.5
Resting V_m (mV)	-70 ± 6	-68 ± 6	-73 ± 5	-69 ± 6	-71 ± 4	$-67 \pm 7^*$
AP threshold (mV)	-49 ± 5	-49 ± 5	-50 ± 5	-48 ± 4	-46 ± 4	-50 ± 3
AP amplitude (mV)	76 ± 8	74 ± 8	78 ± 8	72 ± 10	70 ± 11	74 ± 9
AP half-width duration (ms)	2.0 ± 0.7	2.0 ± 0.6	1.9 ± 1.0	1.8 ± 0.6	2.2 ± 0.4	1.5 ± 0.5
Rate of rise (mV ms^{-1})	66 ± 20	58 ± 13	77 ± 22	59 ± 18	54 ± 18	63 ± 19
AHP (mV)	20 ± 5 ($n = 26$)	22 ± 4 —	17 ± 4 ($n = 14$)	21 ± 5 ($n = 32$)	25 ± 4 ($n = 15$)	17 ± 3 —

Both control and G93A samples were separated using a threshold of 3.25 nS (see Results) to measure the properties of all cells in the sample, low-input conductance (Gn), and high-input conductance cells in the respective cell types. No passive or action potential (AP) parameters were significantly different between the control and G93A motoneurones, with the exception of the high-input conductance G93A resting V_m ($P < 0.05$). This, though, was likely to be due to a larger number of cells in this sample exhibiting spontaneous firing and by excluding all tonically firing cells, the resting V_m was not significantly different. All values are mean ± S.D.

normal motor behaviours (Henneman & Mendell, 1981; Binder *et al.* 1996). Moreover, large motoneurones and their neuromuscular junctions tend to degenerate before small cells in G93A SOD1 mice and, probably, ALS patients (Tandan & Bradley, 1985; Mohajeri *et al.* 1998; Frey *et al.* 2000). We used an input conductance of 3.25 nS to separate both samples (G93A, 16 low- and 17 high-input conductance cells; control, 12 low- and 15 high-input conductance cells).

We assessed the steady-state intrinsic excitability of the cell using the *F–I* function in response to a ramp of injected current (Fig. 3). In G93A motoneurones, the *F–I* gain was similar in both low- and high-input conductance cells, while control high-input conductance cells had lower *F–I* gains than their low-input conductance counterparts (Fig. 4*A*). As a result, the *F–I* gain in the low-input conductance samples was not significantly different between G93A and control motoneurones ($P > 0.1$), whereas the *F–I* gain was significantly larger in the high-input conductance G93A motoneurones ($P = 0.01$). The *F–I* gain was significantly higher in the entire G93A sample (G93A, 0.166 ± 0.087 Hz pA^{-1}; control, 0.115 ± 0.040 Hz pA^{-1}; $P < 0.005$).

The current thresholds for the initial and final spike on the ascending and descending current ramp, respectively, exhibited a similar dichotomy with respect to input conductance. In the high-input conductance samples, the *F–I* functions for G93A motoneurones had a significantly lower initial spike current threshold ($P < 0.05$) and final spike current threshold ($P < 0.02$) compared to control motoneurones (Fig. 4*B* and *C*). *F–I* functions in low-input conductance G93A and control motoneurones, on the other hand, had similar initial spike ($P > 0.5$) and final spike current thresholds ($P > 0.1$) (Fig. 4*B* and *C*). These input conductance-related changes were further supported by an increase in spontaneously firing G93A motoneurones. In high-input conductance G93A motoneurones, 5/17 (29%) exhibited spontaneous firing, whereas none (0/15) of the high-input conductance control cells exhibited this behaviour. However, low-input conductance motoneurones showed similar values for control (3/12; 25%) and G93A (2/16; 13%) cells. In summary, in the high-input conductance G93A motoneurones, not only was *F–I* gain higher, but the current thresholds for the initial and final spikes were decreased.

Differences in persistent currents in low- and high-input conductance cells

The higher *F–I* gains and lower current thresholds in high-input conductance G93A motoneurones compared to control cells were explained by differences in PC_{Na} and $PC_{TTX\text{-}ins}$. The average values of PC_{Na} magnitude for both low- and high-input conductance G93A motoneurones were significantly larger ($P < 0.05$ and $P = 0.005$, respectively) compared to the respective control sample (Fig. 5*A*). In contrast, $PC_{TTX\text{-}ins}$ was only significantly larger in the low-input conductance motoneurones ($P < 0.05$) (Fig. 5*B*). Thus, the input conductance-related changes in the *F–I* gain and current thresholds in G93A cells presumably occurred because the increased $PC_{TTX\text{-}ins}$ offset the increased PC_{Na} in the low-input conductance cells whereas the lack of change in $PC_{TTX\text{-}ins}$ in the high-input conductance cells allowed the increased PC_{Na} to enhance their excitability. The role of PC_{Na} in influencing excitability in high-input conductance G93A cells was supported by a significant correlation between PC_{Na} amplitude and *F–I* gain ($r = 0.72$, $P = 0.001$). Moreover, significant correlations between the onset of PC_{Na} and current thresholds

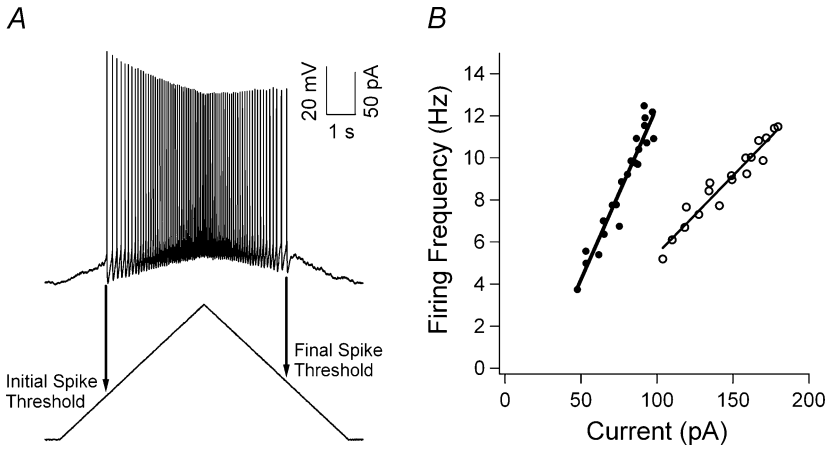

Figure 3. Firing response to a depolarizing current ramp command
A, the voltage response (top) to a current ramp command (bottom) is shown. The current thresholds for the initial and final spike are shown. *B*, the *F–I* relation for a control (○) and G93A (●) cell with the *F–I* gain is plotted for each cell.

were also observed (initial spike threshold, $r = 0.75$, $P < 0.001$; final spike threshold, $r = 0.76$, $P < 0.001$) for the G93A high-input conductance samples. No significant correlations between PC_{Na} and *F–I* parameters were observed in the low-input conductance sample, presumably due to the compensatory change of $PC_{TTX\text{-}ins}$.

Relation between increased PC_{Na} and cell injury

If increased PC_{Na} contributes to cell degeneration in SOD1-mediated ALS, then drugs that suppress PC_{Na} should be neuroprotective. Riluzole is presently the only FDA-approved. drug that significantly prolongs life in human ALS patients (Bensimon *et al.* 1994). In cortical cells, riluzole has recently been shown to effectively block PC_{Na} and decrease neuronal excitability. Furthermore, this blockade occurs at concentrations low enough to be achieved via oral dosage in humans (about 1 μM; Urbani & Belluzzi, 2000). If suppression of PC_{Na} indeed plays an important role in the neuroprotective effect of riluzole in ALS, this drug should also suppress PC_{Na} at low concentrations in motoneurones. Figure 6*A* shows that this is the case, with 0.5 μM riluzole reducing PC_{Na}

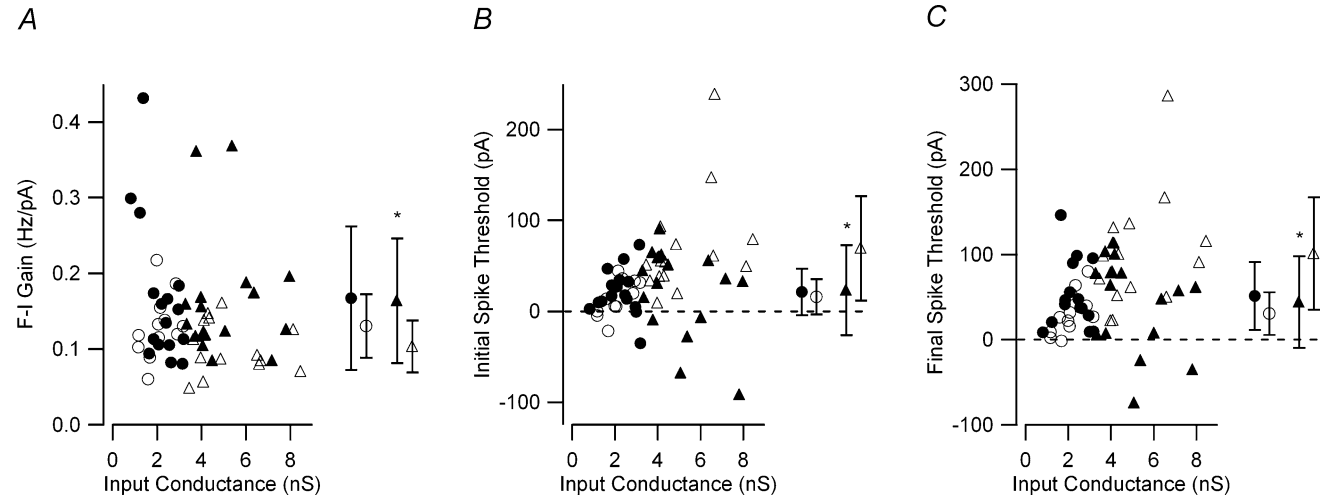

Figure 4. Effect of input conductance on measured firing properties
A, the *F–I* gain for low-input conductance G93A (●) and control (○) and high-input conductance G93A (▲) and control (△) motoneurones is shown. Only the high-input conductance sample had *F–I* gains significantly different. High-input conductance: G93A, 0.164 ± 0.082 Hz pA^{-1}; control, 0.103 ± 0.034 Hz pA^{-1}; low-input conductance: G93A, 0.167 ± 0.095 Hz pA^{-1}; control, 0.130 ± 0.042 Hz pA^{-1}. *B*, similar to the *F–I* gain, input conductance-related changes were observed in the current threshold for the initial spike. High-input conductance: G93A, 23.35 ± 49.49 pA; control, 69.38 ± 57.32 pA; low-input conductance: G93A, 21.33 ± 25.38 pA; control, 15.82 ± 19.61 pA *C*, input conductance-related changes were observed in the current threshold for the final spike. High input conductance: G93A, 43.96 ± 53.8 pA; control, 101.07 ± 65.98 pA; low-input conductance: G93A, 51.52 ± 39.68 pA; control, 30.73 ± 24.86 pA. A significant difference in the current thresholds was only observed in the high-input conductance G93A motoneurones. In each panel on the right side, the mean ± S.D. values are shown; $^*P < 0.05$.

in a non-transgenic (C57BL6 strain) motoneurone. In non-transgenic motoneurones, 0.5 μM riluzole decreased PC_{Na} to approximately 82% of control (64–108%; $n = 5$) and PC to approximately 67% of control (50–114%; $n = 5$). The *F–I* gain was decreased to 84% of the control condition (67–98%; $n = 5$). This decrease in neuronal excitability, PC and PC_{Na}, with the riluzole concentration used (0.5 μM), is unlikely to be due to an increase in outward, or hyperpolarizing, currents (Cao *et al.* 2002).

Riluzole had similar effects on cultured G93A motoneurones. In fact, 0.5 μM riluzole decreased the *F–I* gain, PC and PC_{Na} to levels observed in the control motoneurones (Fig. 6*B* and *C*). In these G93A motoneurones ($n = 8$), the *F–I* gain was reduced from 0.151 ± 0.051 Hz pA^{-1} to 0.084 ± 0.059 Hz pA^{-1} in the presence of 0.5 μM riluzole (Fig. 6*B*). This reduction (56%) in the *F–I* gain was similar to the difference observed between the entire G93A and entire control sample (G93A, 0.166 ± 0.087 Hz pA^{-1}, $n = 33$; control, 0.115 ± 0.040, $n = 27$). The PC in the G93A motoneurones ($n = 8$) was reduced from -83.5 ± 50.4 pA to -46.4 ± 74.1 pA with 0.5 μM riluzole and PC_{Na} ($n = 6$) from -140.2 ± 94.8 pA to -117.6 ± 90.9 pA with 0.5 μM riluzole (Fig. 6*C*). The magnitude of PC_{Na} and PC of the G93A motoneurones in the presence of riluzole (PC_{Na}, -117.6 ± 90.9 pA; PC, -46.4 ± 74.1 pA) was similar to that observed in the entire control sample (PC_{Na}, -78.41 ± 43.32 pA; PC, -58.94 ± 45.10 pA).

Discussion

Although the G93A motoneurones were characterized by increased PC_{Na}, $PC_{TTX\text{-}ins}$ was only significantly larger in low-input conductance motoneurones. A lack of a similar compensatory increase in $PC_{TTX\text{-}ins}$ in high-input conductance cells probably accounted for their increased excitability. These differential changes in excitability may account for the increased vulnerability of large motoneurones to degeneration in ALS (Tandan & Bradley, 1985; Mohajeri *et al.* 1998). Inhibition of PC_{Na} and excitability by riluzole at therapeutic concentrations supports a role for PC_{Na} and hyperexcitability in leading to premature cell death in the G93A SOD1 mice.

Ion channels involved in excitability changes

Because of the considerable variability in excitability and PCs, measurements in many cells were required. We thus sought to isolate only one type of current per cell, PC_{Na}. A decrease in the transient Na^+ current in transfected neuroblastoma cells with the G93A mutation has been reported (Zona *et al.* 1998). However, while decreased transient Na^+ current itself would probably not account for the increased *F–I* gain, this decrease was associated with a depolarizing shift in the inactivation curve (Zona *et al.* 1998). If, as appears likely (Taddese & Bean, 2002), PC_{Na} is very sensitive to the total Na^+ current inactivation, a depolarizing shift could

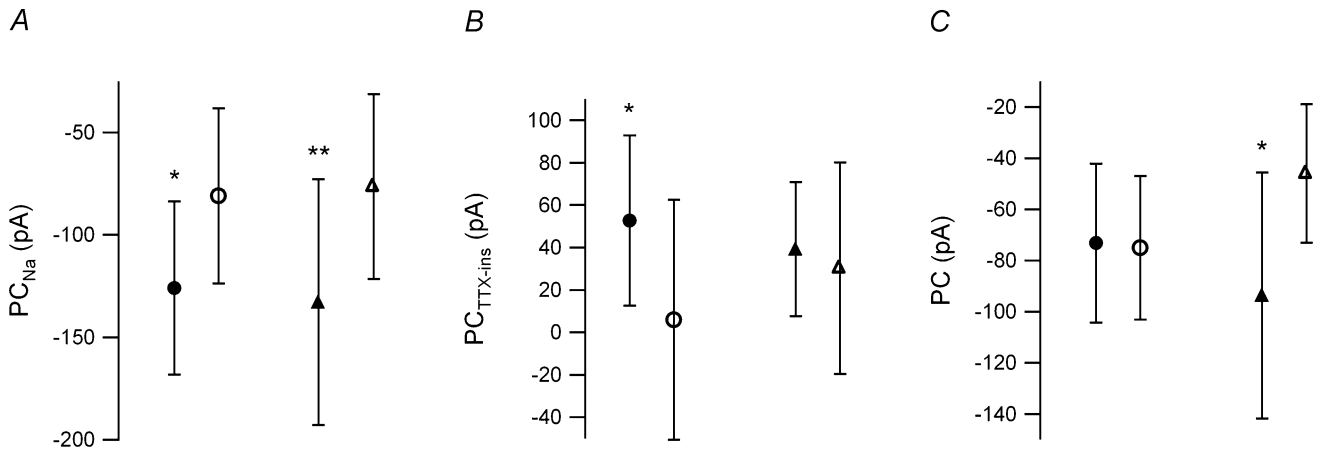

Figure 5. Effect of input conductance on persistent currents
A, G93A low-input conductance (●) and high-input conductance (▲) motoneurones have a significantly larger PC_{Na} than their control counterparts (low-input conductance, ○; high-input conductance Δ). Low input conductance: G93A, -125.88 ± 42.21 pA; control, -80.97 ± 42.76 pA; high input conductance: G93A, -132.88 ± 60.04 pA; control, -76.36 ± 45.15 pA. *B*, the G93A low-input conductance motoneurones had a significantly larger $PC_{TTX\text{-}ins}$ than the control sample, while the high-input conductance samples had similar values. Low input conductance: G93A, 52.70 ± 40.28 pA; control, 5.91 ± 56.55 pA; high input conductance: G93A, 39.26 ± 31.52 pA; control, 30.32 ± 49.9 pA. *C*, only the high-input conductance samples had a significant difference in total PC. The increased PC in the G93A sample was consistent with an increased neuronal excitability in high-input conductance G93A motoneurones. Low input conductance: G93A, -73.18 ± 50.44 pA; control, -75.06 ± 41.88 pA; high input conductance: G93A, -93.63 ± 70.11 pA; control, -46.04 ± 44.71 pA. In each panel $^*P < 0.05$ and $^{**}P = 0.005$.

increase PC_{Na} amplitude. Furthermore, the effect of riluzole in reducing PC_{Na} is likely to involve a hyperpolarizing shift in the Na^+ inactivation curve, therefore decreasing PC_{Na} (Urbani & Belluzzi, 2000).

$PC_{TTX\text{-}ins}$ was probably a mixture of inward and outward currents. As in the present work, it will require a large sample size to accurately correlate each component. Based on the voltage region measured for $PC_{TTX\text{-}ins}$, L-type Ca^{2+} currents, such as CaV1.3 channels, and SK, the calcium-dependent potassium current, are good candidates for the observed changes in $PC_{TTX\text{-}ins}$ (Rekling *et al.* 2000; Goldin, 2001; Powers & Binder, 2001; Xu & Lipscombe, 2001; Heckman *et al.* 2003).

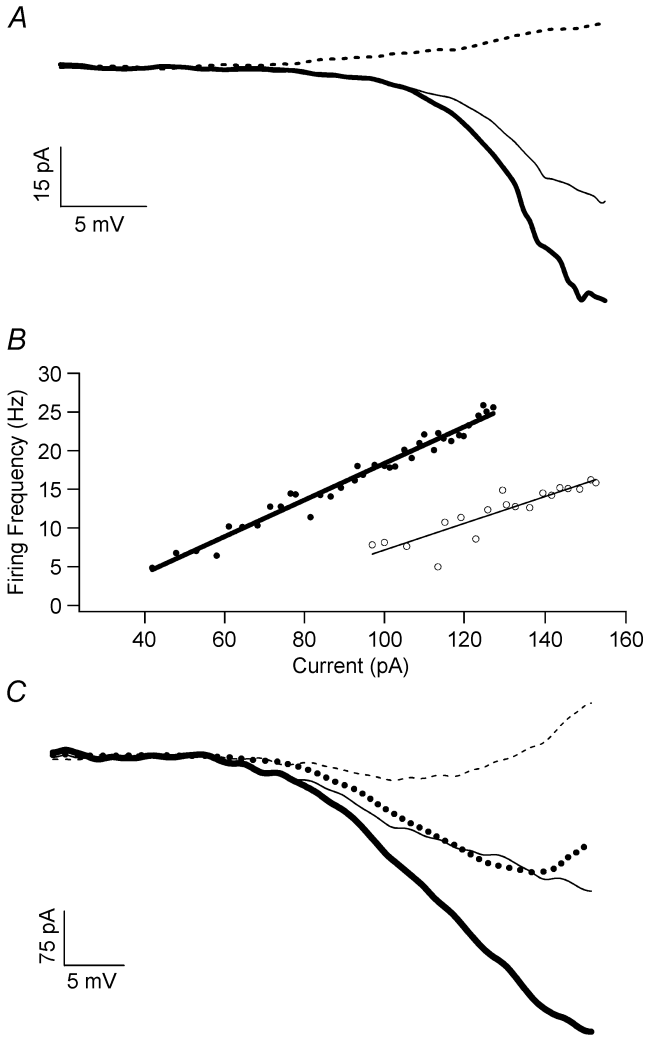

Figure 6. Inhibition of excitability and PC_{Na} by riluzole
A, the *I–V* relations for PC_{Na} are shown for the control condition (thick line) and in the presence of 0.5 μM riluzole (thin line). Riluzole decreased PC_{Na} to approximately 69% of the control value. The *I–V* relation in the presence of TTX is also shown (dashed line). *B*, in the control condition (●), the *F–I* gain to the current ramp stimulus was 0.24 Hz pA^{-1}. The addition of 0.5 μM riluzole (○) decreased the *F–I* gain to 0.174 Hz pA^{-1}. *C*, the *I–V* relations for the control conditions (thick lines) and with 0.5 μM riluzole (thin, dotted lines) are shown with leak subtracted. The decrease in the PC (thin, dotted line) with riluzole was approximately 68% and 87% for PC_{Na} (thick, dotted line).

Potential role of elevated PC_{Na} in the genesis of ALS

Increased excitability may contribute to changes in oxidative stress (Hand & Rouleau, 2002), as well as altered mitochondrial (Heath & Shaw, 2002) and energy metabolism (Ellis *et al.* 2003), and perhaps a chronic state of energy source depletion. Additionally, increased firing rates could allow excessive Ca^{2+} entry and ALS-vulnerable motoneurones possess poor calcium buffering properties compared to ALS-resistant motoneurones (Palecek *et al.* 1999; Vanselow & Keller, 2000). A role for intrinsic excitability in motoneurone degeneration is also suggested by clinical data. ALS patients demonstrated an increased dose–response curve to transcranial stimulation of the motor cortex (Zanette *et al.* 2002), reflecting either increased excitability of corticospinal neurones or spinal motoneurones, or a combination of both.

The foregoing indicates that increases in intrinsic excitability could contribute to excitotoxicity and cell degeneration in ALS. The next step is to consider whether the increased excitability due specifically to aberrant up-regulation of PC_{Na} plays a fundamental role. Two important results support this hypothesis. In ALS patients, motor axons exhibit properties consistent with increased PC_{Na} (Mogyoros *et al.* 1998). Perhaps the most striking result concerns riluzole, which provides significant prolongation of life in human ALS patients and SOD1 mice (Bensimon *et al.* 1994; Gurney *et al.* 1996). Riluzole has a variety of actions, such as inhibition of glutamate release and enhancement of glutamate uptake (Doble, 1996; Dunlop *et al.* 2003). However, at therapeutic concentrations, riluzole also selectively and potently inhibits PC_{Na} and decreases neuronal excitability (Urbani & Belluzzi, 2000). In a motoneurone, the persistent inward current (PIC), which is composed of PC_{Na} and L-type Ca^{2+} current, also affects firing properties (Lee & Heckman, 1998; Heckman *et al.* 2003). The reduction in the *F–I* gain, PIC and PC_{Na} in G93A motoneurones, due to a therapeutic concentration of riluzole (0.5 μM), to levels measured in control motoneurones, suggests that the neuroprotective action of riluzole may be directly related to the inhibition of PC_{Na} and the resulting decrease in excitability.

It should be emphasized that an elevation of PC_{Na} contributes to cell death and is not of course the sole factor. For example, elevated PC_{Na} would increase the excitotoxic effects of (i) elevated glutamate in the spinal cord (Cleveland & Rothstein, 2001), (ii) high concentrations of Ca^{2+}-permeable AMPA receptors on motoneurones (Vandenberghe *et al.* 2000; Van Damme *et al.* 2003) and (iii) poor motoneurone Ca^{2+} buffering capacity (Palecek *et al.* 1999; Vanselow & Keller, 2000).

Culture *versus in vitro* or *in vivo*

Adult turtle motoneurones grown in cell culture de-differentiate and lose their persistent L-type Ca^{2+} currents and, in the majority of cases, the ability to generate sustained rhythmic firing (Perrier *et al.* 2000). The motoneurones in this current study were cultured from the embryonic state and appeared to develop many of the characteristics of young motoneurones. All cells exhibited good rhythmic firing and a large amplitude PC_{Na}. L-type Ca^{2+} currents did not appear to be present in most cells, as administration of TTX usually resulted in a net outward $PC_{TTX\text{-}ins.}$ However, we noted that several low-input conductance control cells did have a net inward $PC_{TTX\text{-}ins}$, which may have been due to L-type Ca^{2+} channels. The absence of net inward currents in G93A motoneurones suggests that L-type Ca^{2+} currents may be suppressed in SOD1 mice as part of the mechanism of adaptation to increased PC_{Na} in low-input conductance cells. This prediction needs to be evaluated in future studies using either slice preparations of juvenile mouse motoneurones (see Carlin *et al.* 2000) or, perhaps, an adult sacral mouse cord preparation based on an *in vitro* rat sacral cord preparation (see Li & Bennett, 2003).

Time course of onset of elevated persistent Na^+ current

While it is unknown how culture development compares to the situation *in vivo*, the lack of differences in the passive cellular properties, consistent culture survival, and recordings well before the onset of symptoms (200 days old) suggest that these cultures represent a presymptomatic state. Therefore, the observed changes in PC_{Na} and excitability may not be as large as other reported aberrations which may be examined just prior to overt symptom onset to end-stage.

The origin of the electrophysiological aberrations observed is presumed to be the motoneurones and their intrinsic properties. The isolation of the cultures to the spinal cord limited the effects of the strongest neuromodulatory input to motoneurones, the monoaminergic input from the brainstem (Rekling *et al.* 2000; Powers & Binder, 2001). In addition, all recordings were obtained with ionotropic synaptic transmission blocked. The absence of neuromuscular junctions in the spinal cultures suggests that the electrophysiological aberrations are initiated in the motoneurone, but it is possible that similar electrophysiological changes in motoneurones will occur as a compensatory mechanism for synaptic transmission failures at the neuromuscular junction (Balice-Gordon *et al.* 2000; Rich *et al.* 2002).

Significance of the difference in excitability of low- and high-input conductance cells

Motor outflow consists of two components, recruitment of motor units and rate modulation of already recruited motor units (Binder *et al.* 1996). If synaptic input is uniformly distributed among the pool of motoneurones innervating a muscle, then the motoneurone *F–I* functions are the only determinants of the recruitment and rate modulation pattern (Heckman & Binder, 1993*a*,*b*). The initial spike threshold determines recruitment and *F–I* gain specifies rate modulation. Normally, because of the size principle of motor unit recruitment, type S motor units are called upon for early recruitment and long periods of steady firing, type FR motor units are fast, moderate force and moderate fatigue-resistant motor units recruited next, and type FF motor units are fast, high force and high fatigue-resistant motor units recruited last (Henneman & Mendell, 1981; Binder *et al.* 1996). Therefore, progressively larger forces are generated by recruitment of progressively larger, higher force and faster motor units. Type S motoneurones have both low-input conductances and small soma sizes, therefore may be expected to degenerate first. However, large motoneurones tend to degenerate before small motoneurones (Tandan & Bradley, 1985; Mohajeri *et al.* 1998). Our results may in part explain this paradox: the increase in excitability and PIC only occurred in high-input conductance cells.

The elevated excitability in high- but not low-input conductance G93A motoneurones constitutes a disruption in the normal hierarchy of electrical excitability. The normal sequence of recruitment, essential for good fatigue resistance in maintained motor behaviours, is critically dependent on the correlations between cell size, input conductance and *F–I* threshold. In fact, most ionotropic synaptic input systems tend to generate larger synaptic currents in high- rather than low-threshold motoneurones (Powers & Binder, 2001).

Predicted symptoms in SOD1 mice and human patients

The observed results could be used to predict symptoms that would occur in mutant SOD1 mice and in human ALS patients if PC_{Na} is elevated and the initial spike current threshold is decreased before the onset of symptoms and overt motoneurone degeneration. The most striking of our results in this regard was the marked decrease in *F–I* threshold of the high-threshold units. Note that in Fig. 4*B*, both low- and high-input conductance G93A motoneurones have similar *F–I* thresholds, whereas in our control cells and in normal motoneurones (Binder *et al.* 1996), high input conductance, presumed type FR or FF motoneurones, have much higher *F–I* thresholds than low-input conductance, presumed type S motoneurones.

Thus FF units would be predicted to be recruited during low force behaviours, such as posture or slow locomotion, which normally rely only on type S motor units. The FF units would in fact be an advantage for strength (and indeed such changes may mask the onset of muscle weakness) but they would produce undue fatigue in prolonged low force outputs. Thus an increase in fatigue and an increase in electromyographic (EMG) activity due to an increase in participating units may be very early signs of ALS.

A slow onset of increased FF excitability may convert the FF muscle fibres to slow twitch properties (Pette & Vrbova, 1999). While the excitability changes in FF motoneurones may be more difficult to detect, these changes would be readily apparent from measurements of recruitment order. Uniquely among CNS neurones, the firing patterns of motoneurones can be routinely assessed in human subjects because of the one-to-one relation between motoneurone firing and that of its muscle fibres (Powers & Binder, 2001). Thus, if motoneurones *in vivo* undergo the same changes in excitability as our cultured motoneurones, then instead of recruitment in order of increasing amplitude of motor unit twitches (measured in humans by an averaging technique; Milner-Brown *et al.* 1973), recruitment should be random.

The preferential increase in excitability of the high-input conductance motoneurones may, alternatively, be explained by differences in specific membrane resistivity. Shifts to higher input resistances, longer AHP durations and lower cell capacitance were observed in axotomized spinal motoneurones (Gustafsson & Pinter, 1984). These aberrations, thought to occur only in type FF motoneurones, indicated that axotomized FF motoneurones de-differentiate (Gustafsson & Pinter, 1984). The differences between our work and the results from the axotomized motoneurones (Gustafsson & Pinter, 1984) may reflect differences between *in vitro* and *in vivo* conditions. In addition to de-differentiation-induced aberrations, the emergence of axon-like processes from the distal dendrites may account for the observed electrophysiological changes in the high-input conductance motoneurones (Rose & Odlozinski, 1998; Rose *et al.* 2001; MacDermid *et al.* 2002; MacDermid *et al.* 2004). It is possible that in our cultures, the high-input conductance motoneurones developed these axon-like distal dendtritic processes that express Na^+ channels, which could contribute to the observed hyperexcitability and increased PC_{Na}. By staining for sodium channel subtypes, specifically those showing persistent kinetics, alterations in the distribution of sodium channels may be revealed (Goldin, 2001).

The aetiology of ALS is heterogeneous. By focusing on SOD1-linked ALS, the motoneurone abnormalities identified in this study can be used to generate predictions about recruitment order and EMG activity that can be tested on this distinct population of ALS patients. Moreover, recruitment order and EMG activity can be measured and tracked in individuals with the SOD1 mutation well before disease onset through disease progression.

References

Anelli R, Dunn ME & Mugnaini E (2000). Unipolar brush cells develop a set of characteristic features in primary cerebellar cultures. *J Neurocytol* **29**, 129–144.

Balice-Gordon RJ, Smith DB, Goldman J, Cork LC, Shirley A, Cope TC *et al.* (2000). Functional motor unit failure precedes neuromuscular degeneration in canine motor neuron disease. *Ann Neurol* **47**, 596–605.

Beers DR, Ho BK, Siklos L, Alexianu ME, Mosier DR, Mohamed AH *et al.* (2001). Parvalbumin overexpression alters immune-mediated increases in intracellular calcium, and delays disease onset in a transgenic model of familial amyotrophic lateral sclerosis. *J Neurochem* **79**, 499–509.

Bennett DJ, Hultborn H, Fedirchuk B & Gorassini M (1998). Synaptic activation of plateaus in hindlimb motoneurons of decerebrate cats. *J Neurophysiol* **80**, 2023–2037.

Bensimon G, Lacomblez L & Meininger V (1994). A controlled trial of riluzole in amyotrophic lateral sclerosis. ALS/Riluzole Study Group. *N Engl J Med* **330**, 585–591.

Binder MD, Heckman CJ & Powers RK (1996). The physiological control of motoneuron activity. In Handbook of Physiology. vol. 12, *Exercise: Regulation and Integration of Multiple Systems*, ed. Rowell LB & Shepherd JT, chapter 1, pp. 1–53. Oxford University Press, New York.

Bruijn LI, Miller TM & Cleveland DW (2004). Unraveling the mechanisms involved in motor neuron degeneration in ALS. *Annu Rev Neurosci* **27**, 723–749.

Cao YJ, Dreixler JC, Couey JJ & Houamed KM (2002). Modulation of recombinant and native neuronal SK channels by the neuroprotective drug riluzole. *Eur J Pharmacol* **449**, 47–54.

Carlin KP, Jiang Z & Brownstone RM (2000). Characterization of calcium currents in functionally mature mouse spinal motoneurons. *Eur J Neurosci* **12**, 1624–1634.

Carriedo SG, Yin HZ & Weiss JH (1996). Motor neurons are selectively vulnerable to AMPA/kainate receptor-mediated injury in vitro. *J Neurosci* **16**, 4069–4079.

Cleveland DW & Rothstein JD (2001). From Charcot to Lou Gehrig: deciphering selective motor neuron death in ALS. *Nat Rev Neurosci* **2**, 806–819.

Crill WE (1996). Persistent sodium current in mammalian central neurons. *Annu Rev Physiol* **58**, 349–362.

Dal Canto MC & Gurney ME (1997). A low expressor line of transgenic mice carrying a mutant human Cu,Zn superoxide dismutase (SOD1) gene develops pathological changes that most closely resemble those in human amyotrophic lateral sclerosis. *Acta Neuropathol (Berl)* **93**, 537–550.

Deng HX, Hentati A, Tainer JA, Iqbal Z, Cayabyab A, Hung WY *et al.* (1993). Amyotrophic lateral sclerosis and structural defects in Cu,Zn superoxide dismutase. *Science* **261**, 1047–1051.

Doble A (1996). The pharmacology and mechanism of action of riluzole. *Neurology* **47**, S233–S241.

Dunlop J, Beal McIlvain H, She Y & Howland DS (2003). Impaired spinal cord glutamate transport capacity and reduced sensitivity to riluzole in a transgenic superoxide dismutase mutant rat model of amyotrophic lateral sclerosis. *J Neurosci* **23**, 1688–1696.

Ellis DZ, Rabe J & Sweadner KJ (2003). Global loss of Na,K-ATPase and its nitric oxide-mediated regulation in a transgenic mouse model of amyotrophic lateral sclerosis. *J Neurosci* **23**, 43–51.

Frey D, Schneider C, Xu L, Borg J, Spooren W & Caroni P (2000). Early and selective loss of neuromuscular synapse subtypes with low sprouting competence in motoneuron diseases. *J Neurosci* **20**, 2534–2542.

Goldin AL (2001). Resurgence of sodium channel research. *Annu Rev Physiol* **63**, 871–894.

Gurney ME (1997). The use of transgenic mouse models of amyotrophic lateral sclerosis in preclinical drug studies. *J Neurol Sci* **152** (Suppl. 1), S67–S73.

Gurney ME, Cutting FB, Zhai P, Doble A, Taylor CP, Andrus PK *et al.* (1996). Benefit of vitamin E, riluzole, and gabapentin in a transgenic model of familial amyotrophic lateral sclerosis. *Ann Neurol* **39**, 147–157.

Gurney ME, Pu H, Chiu AY, Dal Canto MC, Polchow CY, Alexander DD *et al.* (1994). Motor neuron degeneration in mice that express a human Cu,Zn superoxide dismutase mutation. *Science* **264**, 1772–1775.

Gustafsson B & Pinter MJ (1984). Effects of axotomy on the distribution of passive electrical properties of cat motoneurones. *J Physiol* **356**, 433–442.

Hand CK & Rouleau GA (2002). Familial amyotrophic lateral sclerosis. *Muscle Nerve* **25**, 135–159.

Heath PR & Shaw PJ (2002). Update on the glutamatergic neurotransmitter system and the role of excitotoxicity in amyotrophic lateral sclerosis. *Muscle Nerve* **26**, 438–458.

Heckman CJ & Binder MD (1993*a*). Computer simulations of motoneuron firing rate modulation. *J Neurophysiol* **69**, 1005–1008.

Heckman CJ & Binder MD (1993*b*). Computer simulations of the effects of different synaptic input systems on motor unit recruitment. *J Neurophysiol* **70**, 1827–1840.

Heckman CJ, Lee RH & Brownstone RM (2003). Hyperexcitable dendrites in motoneurons and their neuromodulatory control during motor behavior. *Trends Neurosci* **26**, 688–695.

Henneman E & Mendell LM (1981). Functional organization of motoneuron pool and its inputs. In Handbook of Physiology, *The Nervous System, Motor Control*, vol. II part 1, ed. Brooks VB, pp. 423–507. American Physiological Society, Bethesda, MD, USA.

Hounsgaard J, Hultborn H, Jespersen B & Kiehn O (1988). Bistability of alpha-motoneurones in the decerebrate cat and in the acute spinal cat after intravenous 5-hydroxytryptophan. *J Physiol* **405**, 345–367.

Hounsgaard J & Kiehn O (1989). Serotonin-induced bistability of turtle motoneurones caused by a nifedipine-sensitive calcium plateau potential. *J Physiol* **414**, 265–282.

Kong J & Xu Z (1998). Massive mitochondrial degeneration in motor neurons triggers the onset of amyotrophic lateral sclerosis in mice expressing a mutant SOD1. *J Neurosci* **18**, 3241–3250.

Kuo JJ, Fu R, Siddique T & Heckman CJ (2002). Persistent inward currents from SOD1 transgenic mouse cultures. *Abstr Soc Neurosci* 789.7.

Kuo JJ, Schonewille M, Siddique T, Schults AN, Fu R, Bar PR *et al.* (2004). Hyperexcitability of cultured spinal motoneurons from presymptomatic ALS mice. *J Neurophysiol* **91**, 571–575.

Lee RH & Heckman CJ (1998). Bistability in spinal motoneurons in vivo: systematic variations in persistent inward currents. *J Neurophysiol* **80**, 583–593.

Lee RH & Heckman CJ (1999). Paradoxical effect of QX-314 on persistent inward currents and bistable behavior in spinal motoneurons in vivo. *J Neurophysiol* **82**, 2518–2527.

Lee RH & Heckman CJ (2001). Essential role of a fast persistent inward current in action potential initiation and control of rhythmic firing. *J Neurophysiol* **85**, 472–475.

Levi G, Wilkin GP, Ciotti MT & Johnstone S (1989). Preparation of 98% pure cerebellar granule cell cultures. In *A Dissection and Tissue Culture Manual of the Nervous System*, ed. Shahar A, de Vellis J, Vernadakis A & Haber B, pp. 211–214. Alan R. Liss, Inc., New York.

Li Y & Bennett DJ (2003). Persistent sodium and calcium currents cause plateau potentials in motoneurons of chronic spinal rats. *J Neurophysiol* **90**, 857–869.

MacDermid VE, Neuber-Hess MS & Rose PK (2004). The temporal sequence of morphological and molecular changes in axotomized feline motoneurons leading to the formation of axons from the ends of dendrites. *J Comp Neurol* **468**, 233–250.

MacDermid V, Neuber-Hess M, Short C & Rose PK (2002). Alterations to neuronal polarity following permanent axotomy: a quantitative analysis of changes to MAP2a/b and GAP-43 distributions in axotomized motoneurons in the adult cat. *J Comp Neurol* **450**, 318–333.

Milner-Brown HS, Stein RB & Yemm R (1973). The orderly recruitment of human motor units during voluntary isometric contractions. *J Physiol* **230**, 359–370.

Mogyoros I, Kiernan MC, Burke D & Bostock H (1998). Strength-duration properties of sensory and motor axons in amyotrophic lateral sclerosis. *Brain* **121**, 851–859.

Mohajeri MH, Figlewicz DA & Bohn MC (1998). Selective loss of alpha motoneurons innervating the medial gastrocnemius muscle in a mouse model of amyotrophic lateral sclerosis. *Exp Neurol* **150**, 329–336.

Mourelatos Z, Gonatas NK, Stieber A, Gurney ME & Dal Canto MC (1996). The Golgi apparatus of spinal cord motor neurons in transgenic mice expressing mutant Cu,Zn superoxide dismutase becomes fragmented in early, preclinical stages of the disease. *Proc Natl Acad Sci U S A* **93**, 5472–5477.

Palecek J, Lips MB & Keller BU (1999). Calcium dynamics and buffering in motoneurones of the mouse spinal cord. *J Physiol* **520**, 485–502.

Perrier JF & Hounsgaard J (2003). 5-HT2 receptors promote plateau potentials in turtle spinal motoneurons by facilitating an L-type calcium current. *J Neurophysiol* **89**, 954–959.

Perrier JF, Noraberg J, Simon M & Hounsgaard J (2000). Dedifferentiation of intrinsic response properties of motoneurons in organotypic cultures of the spinal cord of the adult turtle. *Eur J Neurosci* **12**, 2397–2404.

Pette D & Vrbova G (1999). What does chronic electrical stimulation teach us about muscle plasticity? *Muscle Nerve* **22**, 666–677.

Pieri M, Albo F, Gaetti C, Spalloni A, Bengtson CP, Longone P*et al.* (2003). Altered excitability of motor neurons in a transgenic mouse model of familial amyotrophic lateral sclerosis. *Neurosci Lett* **351**, 153–156.

Powers RK & Binder MD (2001). Input-output functions of mammalian motoneurons. *Rev Physiol Biochem Pharmacol* **143**, 137–263.

Rao SD & Weiss JH (2004). Excitotoxic and oxidative cross-talk between motor neurons and glia in ALS pathogenesis. *Trends Neurosci* **27**, 17–23.

Reaume AG, Elliott JL, Hoffman EK, Kowall NW, Ferrante RJ, Siwek DF *et al.* (1996). Motor neurons in Cu/Zn superoxide dismutase-deficient mice develop normally but exhibit enhanced cell death after axonal injury. *Nat Genet* **13**, 43–47.

Rekling JC, Funk GD, Bayliss DA, Dong XW & Feldman JL (2000). Synaptic control of motoneuronal excitability. *Physiol Rev* **80**, 767–852.

Rich MM, Wang X, Cope TC & Pinter MJ (2002). Reduced neuromuscular quantal content with normal synaptic release time course and depression in canine motor neuron disease. *J Neurophysiol* **88**, 3305–3314.

Rose PK, MacDermid V, Joshi M & Neuber-Hess M (2001). Emergence of axons from distal dendrites of adult mammalian neurons following a permanent axotomy. *Eur J Neurosci* **13**, 1166–1176.

Rose PK & Odlozinski M (1998). Expansion of the dendritic tree of motoneurons innervating neck muscles of the adult cat after permanent axotomy. *J Comp Neurol* **390**, 392–411.

Rosen DR, Siddique T, Patterson D, Figlewicz DA, Sapp P, Hentati A *et al.* (1993). Mutations in Cu/Zn superoxide dismutase gene are associated with familial amyotrophic lateral sclerosis. *Nature* **362**, 59–62.

Siddique T (1991). Molecular genetics of familial amyotrophic lateral sclerosis. *Adv Neurol* **56**, 227–231.

Siddique T & Lalani I (2002). Genetic aspects of amyotrophic lateral sclerosis. *Adv Neurol* **88**, 21–32.

Taddese A & Bean BP (2002). Subthreshold sodium current from rapidly inactivating sodium channels drives spontaneous firing of tuberomammillary neurons. *Neuron* **33**, 587–600.

Tandan R & Bradley WG (1985). Amyotrophic lateral sclerosis: Part 1. Clinical features, pathology, and ethical issues in management. *Ann Neurol* **18**, 271–280.

Urbani A & Belluzzi O (2000). Riluzole inhibits the persistent sodium current in mammalian CNS neurons. *Eur J Neurosci* **12**, 3567–3574.

Van Damme P, Leyssen M, Callewaert G, Robberecht W & Van Den Bosch L (2003). The AMPA receptor antagonist NBQX prolongs survival in a transgenic mouse model of amyotrophic lateral sclerosis. *Neurosci Lett* **343**, 81–84.

Vandenberghe W, Robberecht W & Brorson JR (2000). AMPA receptor calcium permeability, GluR2 expression, and selective motoneuron vulnerability. *J Neurosci* **20**, 123–132.

Vanselow BK & Keller BU (2000). Calcium dynamics and buffering in oculomotor neurones from mouse that are particularly resistant during amyotrophic lateral sclerosis (ALS)-related motoneurone disease. *J Physiol* **525**, 433–445.

Wong PC, Cai H, Borchelt DR & Price DL (2002). Genetically engineered mouse models of neurodegenerative diseases. *Nat Neurosci* **5**, 633–639.

Xu W & Lipscombe D (2001). Neuronal Ca(V), 1.3alpha 1, L–type channels activate at relatively hyperpolarized membrane potentials and are incompletely inhibited by dihydropyridines. *J Neurosci* **21,** 5944–5951.

Zanette G, Tamburin S, Manganotti P, Refatti N, Forgione A & Rizzuto N (2002). Different mechanisms contribute to motor cortex hyperexcitability in amyotrophic lateral sclerosis. *Clin Neurophysiol* **113**, 1688–1697.

Zona C, Ferri A, Gabbianelli R, Mercuri NB, Bernardi G, Rotilio G *et al.* (1998). Voltage-activated sodium currents in a cell line expressing a Cu,Zn superoxide dismutase typical of familial ALS. *Neuroreport* **9**, 3515–3518.

Acknowledgements

Supported by the National Institute of Neurological Disorders and Stroke NS034382 (C.J.H.), NS37912 and NS021442 (T.S.), the Les Turner ALS Foundation (C.J.H., T.S.), Vena E. Schaff ALS Research Fund (T.S.), Harold Post Research Professorship (T.S.), Herbert and Florence C. Wenske Foundation (T.S.), Ralph and Marian Falk Medical Research Trust (T.S.), Abbott Labs Duane and Susan Burnham Professorship (T.S.).